

Towards Segmentation of Human Teeth Contours in Dental Radiographs Using Active Shape Models

Michael Sprinzl, Walter G. Kropatsch
Vienna University of Technology
Institute of Computer Graphics and Algorithms
Pattern Recognition and Image Processing Group
Vienna, Austria
msprinzl@prip.tuwien.ac.at, krw@prip.tuwien.ac.at

Robert Sablatnig
Vienna University of Technology
Institute of Computer Aided Automation
Computer Vision Lab
Vienna, Austria
sab@caa.tuwien.ac.at

Georg Langs
Medical University of Vienna
Department of Biomedical Imaging and Image-guided Therapy,
Computational Imaging Research Lab
Vienna, Austria
georg.langs@meduniwien.ac.at

Abstract. *We present a framework for segmentation of human teeth contours in dental radiographs. As all humans share the same tooth structure, but show variation in size and morphology, these variations can be modelled using statistical methods. Therefore we propose “Active Shape Models” (ASM) as segmentation approach. ASM are flexible, statistically based models which iteratively move toward structures in images similar to those on which they were trained in advance and consist of a set of corresponding landmarks. Each landmark represents a part of the tooth’s boundary to be located. The training phase of our proposed framework incorporates noise removal, manual segmentation of training images, solving the correspondence problem, aligning the set of training images, and capturing its statistics. For image interpretation, the model of the tooth is placed into the target image. The model parameters are then iteratively adjusted to move the landmarks closer to the contour of the tooth to be segmented. Constraints are applied so that the overall tooth shape to be segmented cannot deform more than the teeth seen in the corresponding training set. Our proposed framework is evaluated using a set of intra-oral dental radiographs containing 60 molars and 70 premolars from 24 patients (22 female, 2 male), taken over a period of ten years.*

1. Introduction

The Department of Oral Surgery of the Bernhard Gottlieb University Clinic for Dentistry (BGUCD) at the Medical University Vienna (MUV) performs more than 2500¹ oral surgery procedures every year. Priorities of the surgical timetable are autotransplantations (“auto” from the Greek meaning for “self”), where the tooth to be transplanted is taken from the same person. In order to determine within the pre-grafting state, which tooth suits best as a donor, and to predict the risk that the grafted tooth will get lost within the post-grafting state, measurements at the dental radiographs of the relevant tooth are performed. As up to now no software exists, which is capable of performing these measurements, they are done manually (see Fig. 1).

Different approaches for segmenting teeth within dental radiograms have been presented in scientific literature so far. In [33], Nomir and Abdel-Mottaleb make use of integral projection. Barboza et al. adopt in [2, 3] a semi-automatic algorithm based on Image Foresting Transform (IFT). The IFT (introduced by Falcão et al. in [17]) defines a robust minimum-cost path in a graph given a set of seed pixels which are the roots of a forest in which the region growth starts.

¹The number of oral surgery procedures is taken from the homepage of the Department of Oral Surgery.

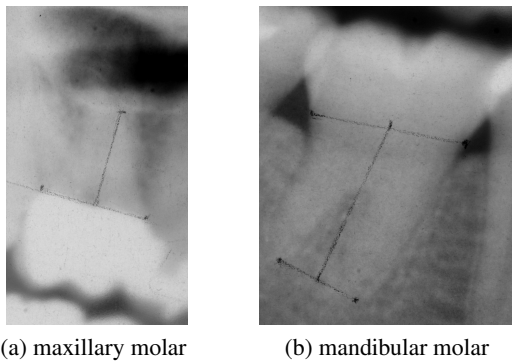


Fig. 1: Examples of performing manual measurements on dental radiographs containing molars in the upper jaw (“Maxilla”) and lower jaw (“Mandible”).

The method recommended by Lin et al. in [25] consists of four stages: image enhancement using an adaptive power law transformation, singularity analysis using local Hölder exponent, tooth recognition using Otsu’s threshold, connected component analysis, and tooth delineation using morphological operations. Morphological operations are also used by Said, Nassar, and Fahmy in [38].

The teeth segmentation pipeline proposed by Frejlichowski and Wanat in [18] consists of three stages: it starts with a morphological opening in order to reduce the noise and to create larger areas of similar intensity range. Afterwards, entropy filtering is applied to detect edges of similar areas. Finally, an iterative watershed region growing constrained by ridge information (see [6] for more details) is done.

Chen and Jain contribute two approaches: In [5] they use Gaussian mixture models (GMM), while in [4] generalized fast marching methods (GFMM) are used. GFMM are special cases of level sets and were introduced by Sethian in [40].

By looking at the papers published so far, it can be concluded that the vast majority uses graph-based and/or morphology-based methods. A drawback that all these methods have in common is that due to noise and artefacts within the image, the segmentation results may not show any similarities to shapes of human teeth at all. This motivates our usage of “Active Shape Models” (ASM) as segmentation approach. ASM, introduced by Cootes and Taylor in [9], are flexible, statistically based models, which iteratively move toward structures in images similar to those on which they were trained in advance. Their application to medical images is shown e. g. in [1, 8, 11, 19, 21, 22, 34, 36, 41, 44].

Overview and contribution. Within this paper we present our proposed teeth segmentation framework consisting of noise reduction, building ASM for molars and premolars using corresponding landmarks on training images, and searching for teeth in target images. Our framework can be used either with MATLAB[®] or GNU Octave.

Within Sec. 2, the medical basics concerning human teeth are presented in a compact manner. Sec. 3 explains our proposed teeth segmentation framework in detail, while the achieved results are presented and discussed in Sec. 4. In Sec. 5, we sum up the conclusions we achieved and address future enhancements.

2. Anatomy of human teeth

According to the definition given by Marcovitch in [27], human teeth are mineralised organs implanted in the jaw, where their visible parts emerge from the bone. The human dentition consists of 20 primary teeth and 32 permanent teeth, which can be classified in incisors, canines, premolars, and molars. Each human tooth has a crown and a root portion. The root portion of the human tooth is implanted into the alveolar jawbone through the periodontal ligament, also called periodontal membrane, and the gum (“Gingiva”), as Nelson explains in [31]. The segmentation is done at this transition between the tooth and its surrounding gingival tissue, which has a size of 2-4 mm, according to Newman et al. in [32].

3. Teeth Segmentation Framework

ASM consists of a sequence of landmarks, each representing corresponding points between similar shapes. During training, a model for molars and premolars is built using the statistics of landmark points within a set of training images. For image interpretation, the model of the tooth to be segmented, is placed into the target tooth image. The tooth model parameters are then iteratively adjusted to move the landmarks closer to the contour of the tooth to be segmented. Constraints are applied so that the overall tooth shape cannot deform more than the teeth seen in the corresponding training set.

3.1. Training phase

The training phase of our proposed teeth segmentation framework incorporates five steps: removing the impulsive noise, manual segmentation of training images, solving the correspondence problem, aligning the training images, and capturing its statistics.

Impulsive Noise Reduction. The dental radiographs we use for training our proposed teeth segmentation framework are analogue X-ray films that were scanned by means of a charge-coupled device (CCD) based X-ray image scanner. This conversion introduces impulsive noise, which appears as random patterns of light and dark pixels (“Salt-and-pepper noise”). Median filtering is used in digital image processing, because it preserves edges while removing impulsive noise. Lin states in [26] that his proposed Adaptive Centre Weighted Median (ACWM) filter “outperforms eight well-accepted alternative median-based filters in terms of both noise suppression and detail preservation. It also provides excellent robustness at various percentages of impulsive noise.” Therefore we use his proposed ACWM filter in order to reduce the impulsive noise in our training images.

Segmentation of Training Images. To speed up the manual segmentation of the training images, we utilise an interactive graph-based image segmentation technique called “Intelligent Scissors”, proposed by Mortensen and Barrett in [29, 30]. The underlying mechanism for Intelligent Scissors is the “Live-Wire” path selection tool. The Live-Wire tool allows the user to interactively select the optimal boundary from a source pixel to a target pixel. To minimise user interaction, seed points are generated automatically along the current active boundary segment via “boundary cooling”. Boundary cooling occurs, when a section of the current portion of the boundary has not changed recently and consequently “freezes”, depositing new seed points, while continuing the optimal boundary expansion.

Solving the Correspondence Problem. After the manual segmentation of the teeth contours, a problem arises when a set of sample points has to be chosen that is placed exactly at corresponding locations within the training set. This problem is known as “correspondence problem”, and is discussed e. g. by Kotcheff and Taylor in [24] and Davies et al. in [15]. One way of solving the correspondence problem is using anatomical landmarks. Kotcheff and Taylor point out in [24] that this manual process is slow, introduces an operator bias and – especially in medical applications – requires expert knowledge of the anatomical structures being dealt with. These problems motivate our search for a method that is capable of solving the correspondence problem without any user intervention.

We use the approach proposed by Davies et al. in [15, 16], which incorporates the Minimum Description Length (MDL) principle (introduced by Rissanen in [37]), for finding pseudo-landmarks automatically within our n_s manually segmented training images.

Aligning a Set of Training Images. In order to be able to compare training shapes containing an equal number of pseudo-landmarks, it is important that the shapes are represented in the same coordinate frame, as Cootes et al. point out in [12]. Therefore, the shapes have to be aligned with respect to a set of axes, in order to remove any kind of variation, which could be attributable to the allowed global transformation. We solve this problem by minimising a sum of squared differences between corresponding pseudo-landmarks on different shapes, which corresponds to a Generalised Procrustes Analysis (GPA) as proposed by Gower in [20], and define x_i as vector containing n_{lm} pseudo-landmarks of the i -th tooth in the training set X such that

$$x_i = (x_{i1}, x_{i2}, \dots, x_{ik}, \dots, x_{in_{lm}}, y_{i1}, y_{i2}, \dots, y_{ik}, \dots, y_{in_{lm}})^T. \quad (1)$$

When two shapes x_i and x_j have to be aligned ($x_i, x_j \in X$), GPA determines a linear transformation of the landmarks in x_j to best conform to the landmarks in x_i . More formally, GPA aligns two shapes by choosing a rotation θ , a scale s , and a translation $t = (t_x, t_y)^T$, mapping x_j onto x_i , so that the resulting dissimilarity measure

$$D = \sum_{k=1}^{n_{lm}} \left(\left(\begin{bmatrix} x_{ik} \\ y_{ik} \end{bmatrix} - M(s, \theta) \begin{bmatrix} x_{jk} \\ y_{jk} \end{bmatrix} - t \right) \left(\begin{bmatrix} x_{ik} \\ y_{ik} \end{bmatrix} - M(s, \theta) \begin{bmatrix} x_{jk} \\ y_{jk} \end{bmatrix} - t \right)^T \right) \quad (2)$$

is minimised, where

$$M(s, \theta) \begin{bmatrix} x_{jk} \\ y_{jk} \end{bmatrix} = \begin{pmatrix} x_{jk} a_x - y_{jk} a_y \\ x_{jk} a_y + y_{jk} a_x \end{pmatrix}, \quad (3)$$

$$\begin{aligned} a_x &= s \cos \theta, \\ a_y &= s \sin \theta. \end{aligned} \quad (4)$$

Computing the derivatives of D shown in Eq. 2 wrt. t_x, t_y, a_x, a_y leads us to A , a set of four linear equations, such that

$$A = \begin{pmatrix} B_1 & -B_2 & n_{lm} & 0 \\ B_2 & B_1 & 0 & n_{lm} \\ B_3 & 0 & B_1 & B_2 \\ 0 & B_3 & -B_2 & B_1 \end{pmatrix} \begin{pmatrix} t_x \\ t_y \\ a_x \\ a_y \end{pmatrix} = \begin{pmatrix} C_1 \\ C_2 \\ C_3 \\ C_4 \end{pmatrix}, \quad (5)$$

where

$$\begin{aligned}
B_1 &= \sum_{k=1}^{n_{lm}} x_{ik}, & B_2 &= \sum_{k=1}^{n_{lm}} y_{ik}, & B_3 &= \sum_{k=1}^{n_{lm}} (x_{ik}^2 + y_{ik}^2), \\
C_1 &= \sum_{k=1}^{n_{lm}} x_{jk}, & C_3 &= \sum_{k=1}^{n_{lm}} (x_{ik}x_{jk} + y_{ik}y_{jk}), \\
C_2 &= \sum_{k=1}^{n_{lm}} y_{jk}, & C_4 &= \sum_{k=1}^{n_{lm}} (x_{ik}y_{jk} - y_{ik}x_{jk}).
\end{aligned} \tag{6}$$

As long as the set of four linear equations shown in Eq. 2 has a non-singular matrix ($\det(A) \neq 0$), it can be solved using standard matrix methods resulting in a single unique solution for t_x, t_y, a_x, a_y . We use an iterative approach for aligning all training shapes within X . It consists of four steps:

1. $\forall x \in X$: align x_i with current \bar{x} .
2. re-calculate \bar{x} using Eq. 7.
3. align current \bar{x} with initial \bar{x} , set current $|\bar{x}| = 1$.
4. $d\bar{x} = \text{current } \bar{x} - \text{previous } \bar{x}$.

Our iterative approach is repeated until $d\bar{x}$ drops under a predefined threshold or the maximum number of iterations is reached.

Capturing the Training Images Statistics. After alignment, all training images are centred and share a common coordinate frame. But one problem remains: each landmark within the training set forms a cloud of corresponding points in a $2n_{lm}$ -dimensional space. To simplify this problem, we apply Principal Component Analysis (PCA) on the aligned shapes in order to reduce their dimensionality. Therefore we calculate the mean shape vector \bar{x} such that

$$\bar{x} = \frac{1}{n_s} \sum_{i=1}^{n_s} x_i \tag{7}$$

and determine the covariance matrix S such that

$$S = \frac{1}{n_s} \sum_{i=1}^{n_s} (x_i - \bar{x})(x_i - \bar{x})^T. \tag{8}$$

Now PCA can be applied on S , resulting in p_k ($k = 1, 2, \dots, 2n_{lm}$) eigenvectors of S such that

$$Sp_k = \lambda_k p_k, \tag{9}$$

where λ_k is the k^{th} corresponding eigenvalue of S (sorted so that $\lambda_k \geq \lambda_{k+1}$).

In order to reduce the dimensionality of the data, the number of eigenvectors (and their corresponding eigenvalues) has to be reduced. Using the fact addressed by Johnson and Wichern in [23] that the variance explained by each eigenvector is equal to the corresponding eigenvalue, the total variance σ^2 is the sum of all eigenvalues, λ_T such that

$$\sigma^2 = \sum_{k=1}^{2n_{lm}} \lambda_k. \tag{10}$$

We choose t , the number of eigenvalues to retain, such that

$$\sum_{i=1}^t \lambda_i \geq f_v \sigma^2, \tag{11}$$

where f_v defines the proportion of the total variance of the training shapes that shall be explained (e. g. 95.45%, which is equivalent to $\pm 2\sigma$ standard deviation of σ^2).

When new shapes are created using the statistics captured above, it is worth noticing that precautions have to be taken in order to ensure that they are similar to the shapes already present within the training data. Cootes et al. name this in [12] as “*creating new allowable shapes*” or “*producing plausible shapes*” that lie within the Allowable Shape Domain (ASD) of the training data. Any shape within the ASD can be approximated by taking \bar{x} and adding a linear combination of the first t eigenvectors multiplied by a vector of weights such that

$$x_{new} \approx \bar{x} + P_t b_t, \tag{12}$$

where $P_t = (p_1; p_2; \dots; p_t)$ is a matrix of the first t eigenvectors, and $b_t = (b_1, b_2, \dots, b_t)^T$ a t -dimensional vector of weights.

3.2. Image Interpretation

Having generated ASM for molars and premolars, we can use them to segment examples of teeth within dental radiographs. This involves - after removing the impulsive noise from the target image, which is done using our proposed ACWM filter - finding shape, scale, and pose parameters which cause the tooth model to coincide with the structures of interest in the dental radiograph containing the tooth to be segmented. According to the definition given by Cootes et al. in [12], an instance of the tooth model is given by

$$X = M(s, \theta)[x] + X_c, \tag{13}$$

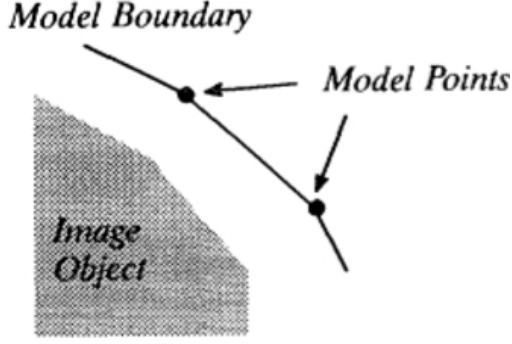


Fig. 2: Part of a model boundary created by connecting the model points (landmarks) approximating to the edge of an image object (Fig. courtesy of [12]).

where $M(s, \theta)[x]$ is a scaling by s and a rotation by θ as defined in Eq. 3, and X_c incorporates the position of the centre of the corresponding tooth model in the image frame such that $X_c = (x_{c1}, x_{c2}, \dots, x_{cn_s}, y_{c1}, y_{c2}, \dots, y_{cn_s})^T$. We use an iterative approach for refining the shape, scale, and pose parameters in order to give a better match to the tooth to be segmented. It consists of three steps:

1. Examine a region around each landmark to calculate the displacements in order to move the landmarks closer to the boundary of the tooth.
2. Use these proposed displacements to calculate adjustments to the shape, scale, and pose parameters of the tooth model.
3. Update the tooth model parameters. By enforcing limits on the shape parameters, global shape constraints can be applied ensuring that the current instance of the tooth model cannot deform more than the teeth seen in the corresponding training set.

Our iterative approach is repeated until either the Sum of Squared Errors (SSE) between the current and the previous instance of the model drops under a predefined threshold or the maximum number of iterations is reached.

Move landmarks closer to the boundary. To start the segmentation process, the user has to place an estimation of the mean shape vector \bar{x} within the dental radiograph containing the tooth to be segmented, which leads to an initial situation similar to the one shown in Fig. 2. As the pseudo-landmarks within an ASM represent the boundaries of image objects, they have to be moved towards the contour of the tooth to be segmented in order to give a better match within

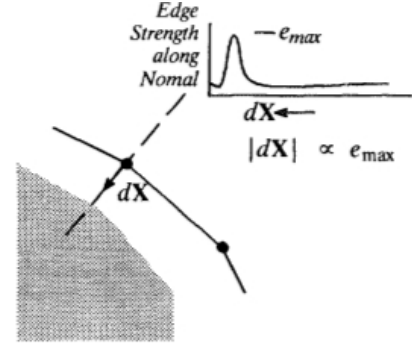


Fig. 3: Suggested movement dX of a model point along a normal to the boundary proportional to the edge strength (Fig. courtesy of [12]).

the next iteration. In the examples Cootes et al. mention in [12], they use an adjustment perpendicular to the model boundary toward the strongest image edge, with a magnitude proportional to the strength of the edge, as illustrated in Fig. 3. This approach results in a vector of adjustments, dX , such that $dX = (dX_1, dX_2, \dots, dX_{n_{lm}}, dY_1, dY_2, \dots, dY_{n_{lm}})^T$.

Calculate adjustments of model parameters. Adjusting the scale and pose parameters of the tooth model means moving the landmarks from their current locations X to the suggested better locations $X + dX$. If we assume that X , the current instance of the tooth model, is centred at X_c with orientation θ and scale s , a set of residual adjustments dx in the local tooth model coordinate frame can be achieved by finding a translation dX_c , a rotation $d\theta$, and a scaling factor $1 + ds$, which best map the landmarks from X to $X + dX$ using Eq. 2-6 such that

$$X + dX = M(s(1 + ds), (\theta + d\theta))[x + dx] + (X_c + dX_c). \quad (14)$$

Inserting Eq. 13 in Eq. 14, eliminating the term X_c , and moving the term dX_c to the left results in

$$M(s, \theta)[x] + dX - dX_c = M(s(1 + ds), (\theta + d\theta))[x + dx], \quad (15)$$

and since $M^{-1}(s, \theta)[\dots] = M(s^{-1}, -\theta)[\dots]$ holds, we obtain

$$dx = M((s(1 + ds))^{-1}, -(\theta + d\theta))[y] - x, \quad (16)$$

where $y = M(s, \theta)[x] + dX - dX_c$. It can be concluded that these adjustments to pose and scale parameters will never be optimal, leaving residual adjustments which can only be satisfied by deforming the shape parameters.

However, it has to be ensured that the tooth model only deforms into shapes consistent with the training set. In order to apply these shape constraints, we transform dx into the parameter space of the model (“tangent space”). This transformation is needed, because dissimilarities between two shapes are not euclidean within the parameter space and therefore cannot be isometrically embedded in a euclidean space, as Wilson et al. point out in [45]. The mapping to tangent space results in db , the changes in model parameters required to adjust the landmarks as closely to dx as allowed. Using Eq. 12, we wish to find db such that

$$x + dx \approx \bar{x} + P_t(b_t + db). \quad (17)$$

Subtracting Eq. 12 from Eq. 17 gives

$$dx \approx P_t db. \quad (18)$$

As the columns of P_t are orthonormal, we are able to calculate $P_t^T = P_t^{-1}$ using the Moore-Penrose pseudo-inverse ([28, 35]), and finally achieve

$$db \approx P_t^T dx. \quad (19)$$

Update the model parameters. Eq. 16 allows us to calculate changes and adjustments dX_c , $d\theta$, and ds , to the scale and pose parameters. Applying Eq. 19, we achieve the updates to the shape parameters db , to adjust the landmarks as closely to dx as allowed. We apply these changes and adjustments in an iterative scheme, such that

$$\begin{aligned} X_c &= X_c + w_t dX_c, \\ \theta &= \theta + w_\theta d\theta, \\ s &= s(1 + w_s ds), \\ b_t &= b_t + W_b db, \end{aligned} \quad (20)$$

where w_t , w_θ , and w_s are scalar weights, while W_b is a diagonal matrix of weights consisting of one weight for each mode, where we choose each weight such that it is proportional to the standard deviation of the variance of its corresponding shape parameter. This allows faster adjustments in modes showing larger shape variations, as Cootes et al. propose in [12]. In order to ensure that the tooth model only deforms into shapes consistent with its training set, we place limits on the values of b_t such that we consider a new shape unacceptable, if the Mahalanobis distance D_m from \bar{x} is greater than D_{max} , such that

$$D_m = \sqrt{\sum_{k=1}^t \left(\frac{b_t^2}{\lambda_k} \right)} > D_{max}. \quad (21)$$

In such a case, b_t has to be rescaled in order to produce a plausible shape using

$$b'_t = b_t \left(\frac{D_{max}}{D_m} \right). \quad (22)$$

Finally, after the scale, pose and shape parameters have been updated, and limits applied where necessary, we move the landmarks from their current locations to the suggested better locations.

4. Results and Discussion

As the development of the segmentation framework that we propose in Sec. 3 is still ongoing due to erroneous results we achieve after calculating the adjustments of the model parameters, we present the results that we obtained so far. The results are evaluated using a set of intra-oral dental radiographs containing 60 molars and 70 premolars from 24 patients (22 female, 2 male), taken over a period of ten years [39], which were scanned using a resolution of 300 dots per inch (dpi) and stored as JPEG-compressed images with a bit depth of 8 bits.

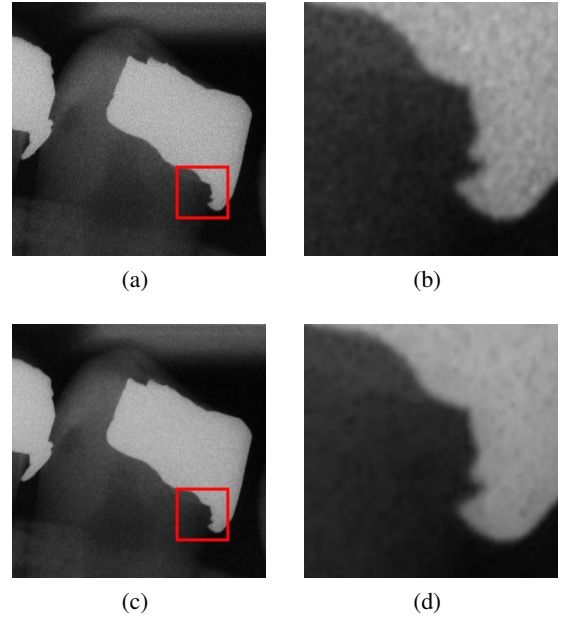


Fig. 4: Dental radiograph of a premolar. The red highlighted areas are zoomed in order to show the amount of impulsive noise present before (a, b) and after filtering (c, d).

Impulsive Noise Reduction. Fig. 4 shows the results of applying impulsive noise reduction using our proposed ACWM filter with five adaptive centre weights and a median filter incorporating a 5-by-5 neighbourhood on a dental radiograph of a premolar.

To evaluate the performance of our ACWM filter, we calculate the mean structural similarity (MSSIM) between the original and the de-noised dental radiograph. The results we achieve can be found in Tab. 1. The definition and a detailed explanation of MSSIM are given by Wang et al. in [43]. We expect our ACWM filter to perform comparable on molars and premolars (null hypothesis, H_0). Running a two-tailed Welch t-test with $\alpha = 0.05$ on our achieved MSSIM values gives $p = 2.287^{-06}$. Therefore we reason that the performance of our proposed ACWM filter is significantly lower on molars. Whether this is due to the different anatomical structure or if another filter parametrisation would have given better results was not evaluated further.

MSSIM	Min. [1]	Median [1]	Mean [1]	Max. [1]
Molar	0.5619	0.7247	0.7414	0.9059
Premolar	0.5973	0.8332	0.8181	0.9267

Tab. 1: Comparison of the MSSIM values we achieve applying our proposed ACWM filtering procedure.

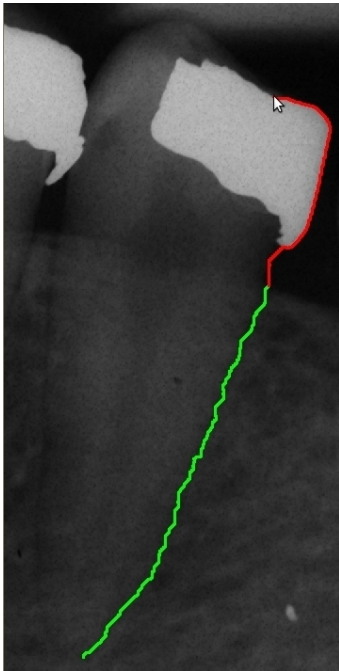


Fig. 5: Screenshot captured during segmentation of a premolar. The segmentation was started at the tip of the premolar and moved upwards in counter-clockwise direction. The green part of the boundary consists of seed points that are already “frozen”, while the red part shows the current active boundary segment proposed by the Live-Wire tool.

Segmentation of Training Images. We use the implementation of the Live-Wire tool published by Hamarneh² et al. in [7] for segmenting the teeth needed to train our proposed teeth segmentation framework. Fig. 5 shows a screenshot captured during manual segmentation of a premolar.

Solving the Correspondence Problem. We use the MDL implementation published by Thodberg in [42] for solving the correspondence problem. We achieve a sequence of n_{lm} pseudo-landmarks placed at corresponding positions within the n_s training shapes, whose arc lengths along the contour are normalised to run from zero to one and whose centres of origin are moved to their respective centres of gravity.

	n_{lm} , [1]	n_{Iter} , [1]	D , [1]
Molar	64	3	2.265^{-06}
	128	3	2.257^{-06}
	256	3	2.265^{-06}
Premolar	64	2	2.429^{-06}
	128	2	2.545^{-06}
	256	2	2.515^{-06}

Tab. 2: Comparison of the alignment iterations and the dissimilarity measure D we achieve after applying our proposed shape alignment procedure.

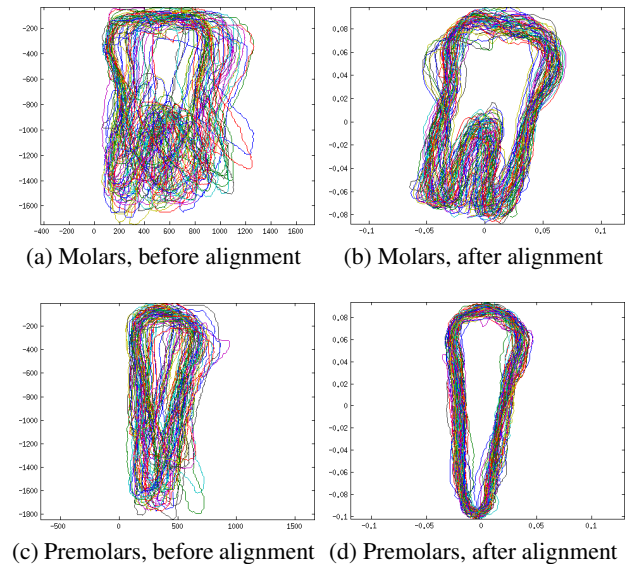


Fig. 6: 60 molar and 70 premolar shapes (with 64 landmarks each) before (left) and after (right) applying our proposed shape alignment procedure.

²Hamarneh’s Live-Wire implementation for MATLAB[®] is available for download at <http://tinyurl.com/osdkr5h/>.

Aligning a Set of Training Images. The alignment of the images needed for training our proposed teeth segmentation framework is done using the GPA approach discussed in Sec. 3. It can be concluded by looking at the results we achieve in Tab. 2 and Fig. 6 that our approach is not only fast (it does not need more than three iterations), but also produces accurately aligned shapes ($D \leq 2.75^{-06}$).

λ_k	$n_{lm} = 64,$ [%]	$n_{lm} = 128,$ [%]	$n_{lm} = 256,$ [%]
1	57.338	57.375	57.391
2	15.348	15.305	15.281
3	8.666	8.675	8.674
4	6.651	6.677	6.666
5	3.184	3.172	3.174
6	1.727	1.720	1.721
7	1.470	1.469	1.475
8	0.830	0.826	0.825
9	0.683	0.688	0.691
$\sum \lambda_k$	95.897	95.907	95.898

(a) Molars

λ_k	$n_{lm} = 64,$ [%]	$n_{lm} = 128,$ [%]	$n_{lm} = 256,$ [%]
1	43.111	43.026	43.082
2	27.793	27.804	27.757
3	8.316	8.373	8.366
4	4.374	4.371	4.363
5	2.978	2.975	2.969
6	2.665	2.674	2.675
7	1.824	1.825	1.830
8	1.683	1.669	1.667
9	1.094	1.090	1.089
10	0.858	0.857	0.858
11	0.626	0.624	0.627
12	0.573	0.578	0.577
$\sum \lambda_k$	95.895	95.866	95.861

(b) Premolars

Tab. 3: Percentage of the variance explained by each λ_k in order to reach 95.45% of the total variance of the captured statistics of 60 molar shapes (above) and 70 premolar shapes (below) containing 64, 128, and 256 pseudo-landmarks.

Capturing the Training Images Statistics. In order to reduce the dimensionality of our training shapes, we capture the image statistics using PCA, as discussed in Sec. 3.

It can be concluded by looking at the results in Tab. 3 that we achieve a huge data compression, as we just need nine eigenvectors in order to reach 95.45% of the total variance of the captured statistics for molars. For premolars, we need only twelve eigenvectors (and their corresponding eigenvalues).

5. Conclusion and Future Work

We presented a framework for segmentation of human teeth contours in dental radiographs using ASM as segmentation approach. We showed the necessary steps to build an ASM (removing the impulsive noise, manual segmentation of training images, solving the correspondence problem, aligning the set of training images, and capturing its statistics). Using our set of dental radiographs containing 60 molars and 70 premolars, we achieved a MSSIM of 0.7414 for molars and 0.8181 for premolars using our proposed ACWM filter. We searched for 64, 128, and 256 corresponding pseudo-landmarks within the manually segmented training images. Aligning them using our proposed GPA approach took three iterations at maximum and produced accurately aligned shapes ($D \leq 2.75^{-06}$). Finally, we were able to reduce the dimensionality of our training images by applying PCA, which resulted in nine remaining eigenvectors for molars and twelve for premolars, in order to reach 95.45% of the total variance of the captured statistics.

For image interpretation, we explained in a theoretical manner how to find shape, scale, and pose parameters, which cause an ASM to coincide with the structures of interest in the dental radiograph containing the tooth to be segmented, as this part of our framework is still in development. Finishing this task has top priority on our list of additions that are foreseen in the future. As soon as image interpretation is working as expected, we plan to incorporate the statistics of local grey levels in regions around each pseudo-landmark. More details regarding local grey levels can be found in [10, 14]. We also consider to enhance our ASM implementation with a multi-resolution approach using image pyramids similar to the one described by Cootes et al. in [13].

Acknowledgements

We would like to thank Dr. Georg D. Strbac from the Department of Oral Surgery of the BGUCD at the MUV for providing the set of dental radiographs used within this paper.

References

- [1] P. D. Allen, J. Graham, D. J. J. Farnell, E. J. Harrison, R. Jacobs, K. Nicopolou-Karayianni, C. Lindh, P. F. van der Stelt, K. Horner, , and H. Devlin. A Generalized Inverse for Matrices. *IEEE Transactions on Information Technology in Biomedicine*, 11(6):601–610, November 2007. 2
- [2] E. B. Barboza and A. N. Marana. A Multibiometric Approach in a Semi Automatic Dental Recognition Using DIFT Technique and Dental Shape Features. In H. Lopes and N. Hirata, editors, *Workshop of Theses and Dissertations (WTD) within the 25th Conference on Graphics, Patterns and Images (SIB-GRAPI '12)*, pages 13–18. SBC, August 2012. 1
- [3] E. B. Barboza, A. N. Marana, and D. T. Oliveira. Semiautomatic Dental Recognition Using a Graph-Based Segmentation Algorithm and Teeth Shapes Features. In A. K. Jain, A. Ross, S. Prabhakar, and J. Kim, editors, *Proceedings of the 5th IAPR International Conference on Biometrics (ICB '12)*, pages 348–353. IEEE Press, March/April 2012. 1
- [4] H. Chen. *Automatic Forensic Identification based on Dental Radiographs*. PhD thesis, Michigan State University, East Lansing, MI, USA, 2007. 2
- [5] H. Chen and A. K. Jain. Dental Biometrics: Alignment and Matching of Dental Radiographs. *IEEE Transactions on Pattern Analysis and Machine Intelligence*, 27(8):1319–1326, August 2005. 2
- [6] L. Chen, M. Jiang, and J. Chen. Image Segmentation Using Iterative Watershedding Plus Ridge Detection. In *Proceedings of the 16th IEEE International Conference on Image Processing (ICIP '09)*, pages 4033–4036. IEEE Press, November 2009. 2
- [7] A. Chodorowski, U. Mattsson, M. Langille, and G. Hamarneh. Color Lesion Boundary Detection using Live Wire. In *Proceedings of SPIE Medical Imaging 2005: Image Processing*, volume 5747, pages 1589–1596. SPIE, April 2005. 7
- [8] T. F. Cootes, A. Hill, C. J. Taylor, and J. Haslam. The Use of Active Shape Models for Locating Structures in Medical Images. *Image and Vision Computing*, 12(6):355–365, July 1994. 2
- [9] T. F. Cootes and C. J. Taylor. Active Shape Models – “Smart Snakes”. In *Proceedings of the 3rd British Machine Vision Conference (BMVC '92)*, pages 266–275. Springer-Verlag, September 1992. 2
- [10] T. F. Cootes and C. J. Taylor. Active Shape Model Search Using Local Grey-Level Models – A Quantitative Evaluation. In *Proceedings of the 4th British Machine Vision Conference (BMVC '93)*, pages 639–648. BMVA Press, September 1993. 8
- [11] T. F. Cootes and C. J. Taylor. Statistical Models of Appearance for Medical Image Analysis and Computer Vision. In *Proceedings of SPIE Medical Imaging 2001: Image Processing*, volume 4322, pages 236–248. SPIE, February 2001. 2
- [12] T. F. Cootes, C. J. Taylor, D. H. Cooper, and J. Graham. Active Shape Models – Their Training and Application. *Computer Vision and Image Understanding*, 61(1):38–59, January 1995. 3, 4, 5, 6
- [13] T. F. Cootes, C. J. Taylor, and A. Lanitis. Multi-Resolution Search with Active Shape Models. In *Proceedings of the 12th IAPR International Conference on Pattern Recognition (ICPR '94)*, volume 1, pages 610–612. IEEE Press, October 1994. 8
- [14] T. F. Cootes, C. J. Taylor, A. Lanitis, D. H. Cooper, and J. Graham. Building and Using Flexible Models Incorporating Grey-Level Information. In *Proceedings of the 4th International Conference on Computer Vision (ICCV '93)*, pages 242–246. IEEE Press, May 1993. 8
- [15] R. H. Davies, T. F. Cootes, and C. J. Taylor. A Minimum Description Length Approach to Statistical Shape Modelling. In *Proceedings of the 17th International Conference on Information Processing in Medical Imaging (IPMI '01)*, pages 50–63. Springer-Verlag, June 2001. 3
- [16] R. H. Davies, C. J. Twining, T. F. Cootes, J. C. Watterton, and C. J. Taylor. A minimum description length approach to statistical shape modelling. *IEEE Transactions on Medical Imaging*, 21(5):525–537, May 2002. 3
- [17] A. X. Falcão, J. Stolfi, and R. de Alencar Lotufo. The Image Foresting Transform: Theory, Algorithms, and Applications. *IEEE Transactions on Pattern Analysis and Machine Intelligence*, 26(1):19–29, January 2004. 1
- [18] D. Frejlichowski and R. Wanat. Extraction of Teeth Shapes from Orthopantomograms for Forensic Human Identification. In P. Real, D. Diaz-Pernil, H. Molina-Abril, A. Berciano, and W. G. Kropatsch, editors, *Computer Analysis of Images and Patterns*, volume 6855 of *Lecture Notes in Computer Science*, pages 65–72. Springer-Verlag, 2011. 2
- [19] B. van Ginneken, M. B. Stegmann, and M. Loog. Segmentation of anatomical structures in chest radiographs using supervised methods: a comparative study on a public database. *Medical Image Analysis*, 10(1):19–40, February 2006. 2
- [20] J. C. Gower. Generalized Procrustes Analysis. *Psychometrika*, 40(1):33–51, March 1975. 3
- [21] T. J. Hutton, S. Cunningham, and P. Hammond. An evaluation of Active Shape Models for the automatic identification of cephalometric landmarks. *European Journal of Orthodontics*, 22(5):499–508, October 2000. 2
- [22] T. J. Hutton, P. Hammond, and J. C. Davenport. Active Shape Models for Customised Prosthesis Design. In *Proceedings of the 7th Joint European Conference on Artificial Intelligence in Medicine and Medical Decision Making (AIMDM '99)*, LNAI 1620, pages 448–452. Springer, June 1999. 2

- [23] R. A. Johnson and D. W. Wichern. *Applied Multivariate Statistical Analysis*. Prentice Hall, 6th edition, March 2007. 4
- [24] A. C. W. Kotcheff and C. J. Taylor. Automatic Construction of Eigenshape Models by Direct Optimization. *Medical Image Analysis*, 2(4):303–314, December 1998. 3
- [25] P. L. Lin, P. Y. Huang, P. W. Huang, H. C. Hsu, and C. C. Chen. Teeth Segmentation of Dental Periapical Radiographs Based on Local Singularity Analysis. *Computer Methods and Programs in Biomedicine*, 113(2):433–445, February 2014. 2
- [26] T.-C. Lin. A new Adaptive Centre Weighted Median Filter for Suppressing Impulsive Noise in Images. *Information Sciences*, 177(4):1073–1087, February 2007. 3
- [27] H. Marcovitch. *Black's Medical Dictionary*. A&C Black Publishers, 42nd edition, September 2009. 2
- [28] E. H. Moore. On the Reciprocal of the General Algebraic Matrix. *Bulletin of the American Mathematical Society*, 9(26):394–395, September 1920. 6
- [29] E. N. Mortensen and W. A. Barrett. Intelligent Scissors for Image Composition. In *Proceedings of the 22nd Annual Conference on Computer Graphics and Interactive Techniques (SIGGRAPH '95)*, pages 191–198. ACM, December 1995. 3
- [30] E. N. Mortensen and W. A. Barrett. Interactive Segmentation with Intelligent Scissors. *Graphical Models and Image Processing*, 60(5):349–384, September 1998. 3
- [31] S. J. Nelson. *Wheeler's Dental Anatomy, Physiology and Occlusion*. Saunders, 9th edition, June 2009. 2
- [32] M. G. Newman, H. Takei, F. A. Carranza, and P. R. Klokkevold. *Carranza's Clinical Periodontology*. Saunders, 10th edition, July 2006. 2
- [33] O. Nomir and M. Abdel-Mottaleb. A System for Human Identification From X-ray Dental Radiographs. *Pattern Recognition*, 38(8):1295–1305, August 2005. 1
- [34] A. D. Parker, A. Hill, C. J. Taylor, T. F. Cootes, X. Y. Jin, and D. G. Gibson. Application of point distribution models to the automated analysis of echocardiograms. In *Proceedings of the 21st International Conference on Computers in Cardiology (CinC '94)*, pages 25–28. IEEE Press, September 1994. 2
- [35] R. Penrose. A Generalized Inverse for Matrices. *Proceedings of the Cambridge Philosophical Society*, 51(3):406–413, July 1955. 6
- [36] A. L. Redhead, A. C. W. Kotcheff, C. J. Taylor, M. L. Porter, and D. W. L. Hukins. An Automated Method for Assessing Routine Radiographs of Patients with Total Hip Replacements. *Proceedings of the Institution of Mechanical Engineers, Part H: Journal of Engineering in Medicine*, 211(2):145–154, January 1997. 2
- [37] J. Rissanen. Modeling by shortest data description. *Automatica*, 14(5):465–471, September 1978. 3
- [38] E. H. Said, D. E. M. Nassar, and G. Fahmy. Teeth Segmentation in Digitized Dental X-Ray Films Using Mathematical Morphology. *IEEE Transactions on Information Forensics and Security*, 1(2):178–189, June 2006. 2
- [39] B. Schwinner. Vertical Bone Height and Apex Growth of Autografted Teeth. Master's thesis, Medical University Vienna, Bernhard Gottlieb University Clinic for Dentistry, Department of Oral and Maxillofacial Surgery, May 2007. 6
- [40] J. A. Sethian. A Fast Marching Level Set Method for Monotonically Advancing Fronts. *Proceedings of the National Academy of Sciences of the United States of America*, 93(4):1591–1595, February 1996. 2
- [41] S. Solloway, C. E. Hutchinson, J. C. Waterton, and C. J. Taylor. The use of Active Shape Models for making thickness measurements of articular cartilage from MR images. *Magnetic Resonance in Medicine*, 37(6):943–952, June 1997. 2
- [42] H. H. Thodberg. Minimum Description Length Shape and Appearance Models. In *Proceedings of the 18th International Conference on Information Processing in Medical Imaging (IPMI '03)*, pages 51–62. Springer-Verlag, July 2003. 7
- [43] Z. Wang, A. C. Bovik, H. R. Sheikh, and E. P. Simoncelli. Image Quality Assessment: From Error Visibility to Structural Similarity. *IEEE Transactions on Image Processing*, 13(4):600–612, April 2004. 7
- [44] P. A. Widhalm. Automatic Assessment of the Knee Alignment Angles on Full-limb Radiographs. Master's thesis, Vienna University of Technology, Institute of Computer Aided Automation, Pattern Recognition and Image Processing Group, October 2008. 2
- [45] R. C. Wilson, E. R. Hancock, E. Pekalska, and R. P. W. Duin. Spherical and Hyperbolic Embeddings of Data. *IEEE Transactions on Pattern Analysis and Machine Intelligence*, 36(11):2255–2269, November 2014. 6